ELSEVIER

Polymer 42 (2001) 5871–5883

polymer

www.elsevier.nl/locate/polymer

# A study on solid-state drawn fibers of polyethylene by confocal Raman microspectrometry: evaluation of the orientation profiles of amorphous and crystalline phases across the fiber section

C. Fagnano[a], M. Rossi[a], R.S. Porter[b,‡], S. Ottani[c,*]

[a]*Dipartimento di Biochimica — Sez. Chimica, Università di Bologna, Via Selmi 2, 40126 Bologna, Italy*
[b]*Polymer Science and Engineering Department, University of Massachusetts, Amherst, MA 01003, USA*
[c]*C.N.R. — Istituto LAMEL, Via Gobetti 101, 40129 Bologna, Italy*

Received 1 May 2000; received in revised form 1 December 2000; accepted 6 December 2000

**Abstract**

Polarized Raman macrospectrometry and confocal Raman microspectrometry have been used to evaluate the uniaxial draw of polyethylene (PE) at a draw ratio of ~6. The draw was conducted by solid-state extrusion. The PE samples tested were synthesized to different molecular weights by slurry and gas phase processes at different temperatures. Raman spectra offer an important evaluation of draw, with bands identifiable for each: the amorphous, crystalline and interphase regions of the morphology. Such an interphase is preferentially located at the crystallite fold surface boundary and it has been associated with the presence of chain loops and entangled chain segments in this region. Orientations of the different phases are estimated by measuring the depolarization factors of the corresponding bands. Further, by confocal Raman microspectrometry, profiles of orientation across the fiber have been identified, by focusing the laser beam at different depths in the drawn PE. It was found that the crystalline component orients along the draw direction, while, across the fiber section, the interphase and the liquid-like amorphous component display preferred orientation normal to the draw direction. Correlations among orientation profiles, synthesis conditions and reactor powder ductility are discussed. Orientation profiles have been compared to the deformation profiles obtained by the displacement of pre-imprinted ink marks on the drawn fibers. A possible interpretation of the orientation profiles is attempted in terms of the relevant modes of deformation and alignment of chain segments in the different phases. The Raman results, in combination with wide angle X-ray analysis reveal steps in the drawn process that have implications for understanding the draw of PE and possibly for the general process of 'necking' on draw of semicrystalline thermoplastics. 

*Keywords*: Polyethylene fibers; Confocal Raman spectroscopy; Orientation profiles

## 1. Introduction

Polymeric fibers make up a class of products of high technological interest. On a weight basis, these fibers can display a set of physical and mechanical properties comparable or even superior to steel products. Among polymeric fibers, those made by ultra-high molecular weight polyethelene (UHMWPE) can be distinguished by their ability to provide, at a low cost, a unique combination of low specific weight with high tensile moduli and strength. These properties can prove particularly useful in a range of applications like in the anchorage of oilrigs, towing ropes, composite reinforcement and in bulletproof vests.

On a molecular basis, the achievement of high tensile moduli has been related to the extension and parallel alignment of polymeric chains so that the macroscopic elongation of the fiber can be transferred to the deformation of stiff covalent bonds and bond angles along the molecular backbone. Such a process can be greatly affected by the presence of entanglements among polymeric chains. Entanglements can act as friction centers and temporary junctions hindering and stopping the extension and the alignment of the chain segments [1,2]. The maximum achievable draw ratio is expected to depend strongly on the degree of entanglements. However, entanglements can also provide effective stress-transfer connections between different chains and can improve the efficiency of draw [3]. For solid state draw (SSD) of semicrystalline polymers, it has been suggested that, especially in the initial stages of the draw process, higher contents of entanglements can lead

* Corresponding author. Fax: +39-051-639-9216.
*E-mail address:* ottani@lamel.bo.cnr.it (S. Ottani).
‡ Deceased author.

0032-3861/01/$ - see front matter 
PII: S0032-3861(00)00913-7

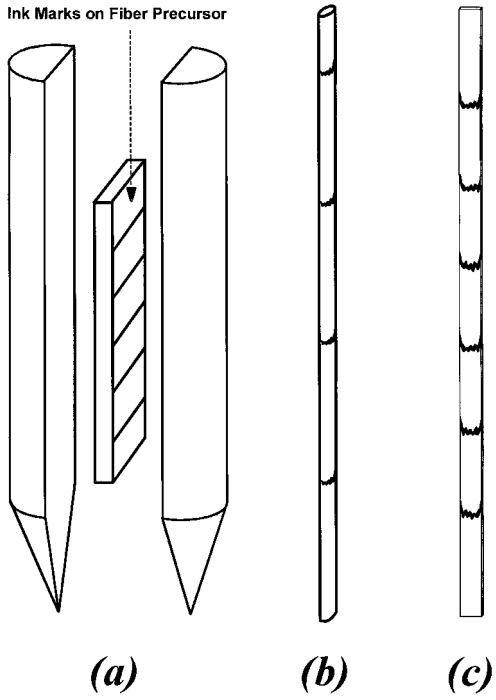


Fig. 1. (a) Split billet assembly. (b) Coextruded fiber from reactor powders.(c) Coextruded film from solution grown single crystal mats.

to more significant strain of the amorphous phase and to higher crystallite alignment along the applied stress field [4].

Studies on the solid state deformation of semicrystalline PE have shown that the flow profiles corresponding to the changes in the strain rate across the fiber section can take different shapes, from simple flat or concave patterns to more complex W-shaped patterns [5,6]. Differences in the strain rate along the fiber cross-section should correspond to changes in the orientations of the crystalline and amorphous phases at different depths below the fiber surface. Such data can be relevant for a better understanding of the effects of entanglements on the mechanism of plastic deformation.

Several techniques have been used to measure orientation profiles on draw. Thin sections of the specimens can be investigated by X-ray diffraction [7] or transmission electron microscopy (TEM) to estimate orientation at different depths. Attenuated total reflection infrared spectroscopy (FT-IR/ATR) [8] or multiple internal reflection infrared spectroscopy (MIR) [9] are more suitable and non-destructive techniques, but the range of achievable depths is limited to few μm [9]. Polarized Raman spectroscopy has been employed to measure the orientation function in PE fibers [7,10–13]. The technique is easy to implement and its non-destructive character prevents unwanted modifications in the oriented phases because of preliminary sample treatment. However, as such, this technique cannot be used for orientation profiling since the measured scattering is limited to a thin surface layer of the specimen [9]. In contrast, confocal Raman microspectrometry (CRM) has been successfully used for the depth profiling of physical and chemical parameters in several inorganic, polymeric and biological systems [14–16]. However, a survey of the recent literature does not show that this technique has ever been employed to investigate orientation profiles in polymer fibers. Actually, scattered intensities decrease significantly on moving the focal plane at increasing depths into the specimen. This leads to unreliable values of the depolarization factors required to compute orientation functions. Additional problems arise from optical inhomogeneities in the sample, which can modify the polarization of the scattered beam. Nevertheless, as reported in the following sections, intensity ratios measured at different depths by a particular experimental assembly still show a correlation with depolarization factors. Thus, in this work an attempt is made to use such values of the intensity ratios to estimate the orientation profiles of the crystalline and amorphous phases across the fiber section.

The samples studied in this work were a set of UHMWPE fibers obtained by solid-state coextrusion of nascent reactor powders. It was reported that, under particular conditions, synthesis could provide UHMWPE powders that can be directly drawn [1]. This is a possible indication of a low degree of entanglement in some reactor powders. Such a low degree of entanglement can be preserved by maintaining the process temperature below the melting point through the several stages of conversion of reactor powders into fibers. The SSD of UHMWPE reactor powders has been previously studied with the aim to correlate structural and morphological changes induced by draw with specific sets of synthesis conditions [4,17–19]. Such studies have focused on the identification of reliable parameters to estimate powder ductility prior to draw. Possible correlations between the nascent degree of entanglements and synthesis conditions were also investigated [20–24]. These studies showed that coextrusion of reactor powders at a draw ratio of about six leads to specimens, whose physical and structural properties are still related to the initial morphology and to the persistence of nascent chain arrangements, stemming from specific combinations of synthesis conditions [4,25]. Thus, correlations between synthetic conditions and orientation profiles of the corresponding SSD fibers can provide information on the local efficiency of draw. Such data might prove relevant to estimate the influence of entanglements on the development of the stress field along the fiber section during the coextrusion stage. They can also be useful to investigate the sequence of molecular processes at ever-higher draw.

## 2. Experimental

UHMWPE samples were synthesized at Union Carbide Corporation. Synthesis was performed by Ziegler–Natta heterogeneous catalysis, either by slurry or gas-phase process. Details of the syntheses have been given in Ref. [21]. Fibers have been obtained by pressing reactor powders

Table 1
PE reactor powders characterization

| Sample identification | $\bar{M}_v \times 10^{-6}$[a] | $\bar{l}$ (Å), DSC[b] | $\alpha_b$ in %, Raman[c] | Cryst.%, DSC[d] | hhw, DSC[e] | EDR[f] | $TDR_{max}$ (135°C)[g] | Tensile modulus (GPa) |
|---|---|---|---|---|---|---|---|---|
| Sl30-05.9 | 5.95 | 303 | – | 67.2 | 2.81 | 5.7 | 9 | – |
| Sl30-12.4 | 12.4 | 296 | 18 | 66.8 | 2.79 | 5.7 | 6 | – |
| Sl85-00.9 | 0.93 | – | – | 70.2 | 2.30 | | – | – |
| Sl85-02.0 | 2.00 | 211 | – | 67.6 | 2.30 | 5.7 | 85 | 57 |
| Sl85-04.8 | 4.80 | 206 | 5 | 67.8 | 2.30 | 5.8 | 98 | 75 |
| Gp85-00.2 | 0.16 | 202 | – | 63.2 | 3.32 | 5.8 | 19 | – |
| Gp85-01.0 | 0.96 | 200 | 14 | 64.7 | 3.32 | 5.8 | 22 | – |

[a] Molecular weight viscosity average.
[b] Average lamellar thickness, computed by the Thompson–Gibbs equation.
[c] Relative amount of interphase.
[d] Percent crystallinity computed by DSC enthalpies of melting.
[e] DSC melting peak width at half height measured at 0.4°C/min.
[f] Draw ratio after coextrusion.
[g] Total draw ratio (TDR) is the extrusion draw ratio (EDR) multiplied by the final tensile draw ratio.

at 150 kg $cm^{-2}$ under vacuum at 120°C. Strips cut from the compressed plates were sandwiched between the two halves of a cylindrical split billet of high-density PE (see Fig. 1a) and the billet was coextruded through a bronze conical die of 20° entrance angle. Coextrusion temperature was 120°C and the extruded draw ratio (EDR) was near six. Values of EDR as well as deformation profiles obtained in the coextrusion stage were estimated by the displacement of ink marks pre-imprinted on the UHMWPE strip (Fig. 1a). To allow comparisons among specimens obtained by different synthesis processes, identical conditions were used for all samples in the whole coextrusion process. Ductility of the reactor powders have been estimated by the maximum total draw ratio (TDR), viz. the maximum achievable draw ratio measured after drawing the coextruded fibers in free space [23]. Values of TDR were computed as the product of the draw ratios in the two steps. Table 1 reports the relevant parameters of the synthesis processes and the mechanical properties of the samples investigated in this work.

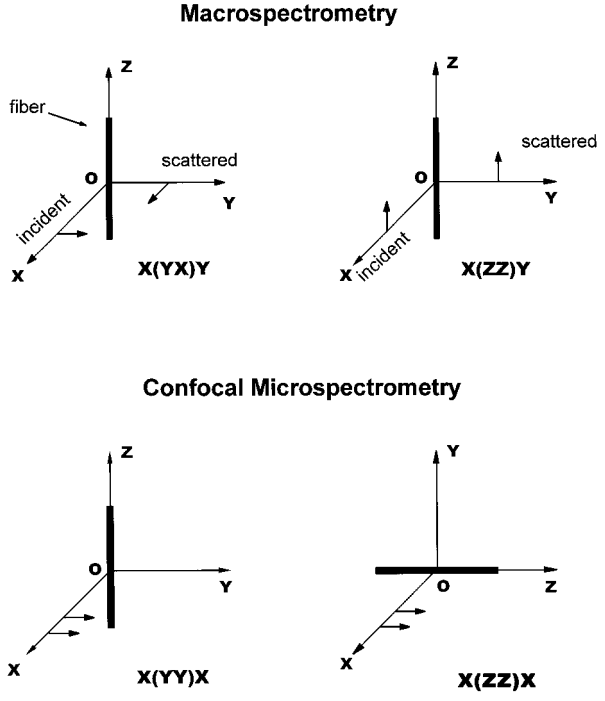


Fig. 2. Scattering geometries. Confocal microspectrometry is performed in backscattering.

Coextruded fiber specimens were optically opaque with an elliptic cross section and a rather irregular surface (Fig. 1b). Sample width ranged between 2 and 3 mm and thickness between 450 and 500 μm. Samples have been investigated by Raman macrospectroscopy, CRM and wide-angle X-ray scattering (WAXS).

For checking possible experimental biases, Raman measurements were performed also on a different type of fiber, obtained by coextrusion at EDR = 6 of solution grown single crystal mats [26]. In this case, a thin film with a flat and very smooth surface is obtained (Fig. 1c).

### 2.1. Raman macrospectroscopy

Raman spectra were collected using a Jasco NR-1100 double monochromator (focal length of 1000 mm, holographic diffraction grating of 1800 lines/mm) equipped with a Coherent Radiation (Innova 90) argon ion laser, the 488.0 nm line being used for excitation. The sample was irradiated from below by a laser beam of 180–200 mW, the 90° scattering being collected. The following instrumental settings were used: spectral slit widths of 5 $cm^{-1}$, scanning speed 60 $cm^{-1}$/min and time constant 0.5 s. The external reference frame is *OXYZ*, where the fiber specimen axis (the draw direction) is always parallel to *OZ*. *OX* is in the direction of the incident laser beam, *OY* in the scattered beam direction (Fig. 2, top). To reduce grating polarization effects, a crystal quartz scrambler was inserted immediately before the entrance slit of the monochromator. The rotation

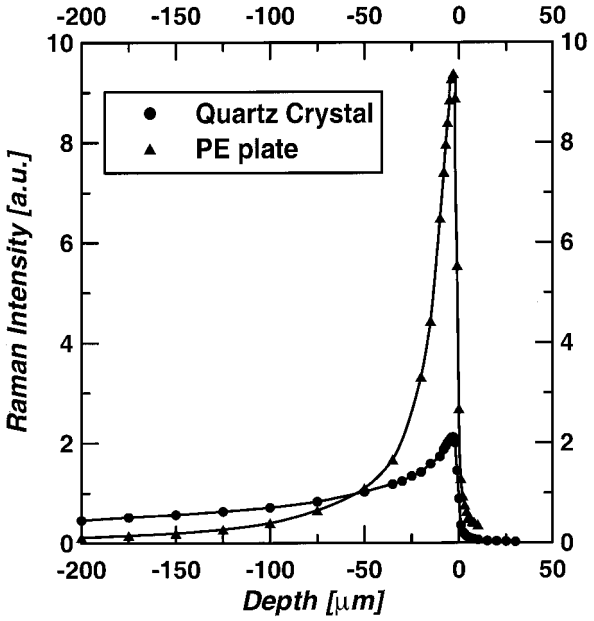


Fig. 3. Depth resolution. Scattered intensities in arbitrary units at different focusing depths: maximum values of intensities are at −2.5 μm, where the scattering volume is completely filled by the sample.

of the polarization plane of the incident radiation was obtained with a half-wave plate. According to Porto's nomenclature, the scattering geometry can be described by a four-letter notation: $A(BC)D$, where $A$, $B$, $C$, and $D$ stand for one of the axis of the external reference frame, $X$, $Y$, or $Z$. $A$ is the direction of the laser beam, $B$ the polarization of the laser, $C$ the direction of the polarization analyzer and $D$ the direction of view (the direction for the collection of the scattered intensities). The degree of chain orientation along the draw direction can be estimated by depolarization factors $R$, the ratio of the peak intensities in the $X(YX)Y$ and $X(ZZ)Y$ orientations ($R = I_{X(YX)Y}/I_{X(ZZ)Y}$) [12]. Inhomogeneities at the specimen surface have been accounted for, by taking measurements at five different spots for each fiber and averaging the resulting spectra. For all Raman peaks and for each set of measurements, the largest difference between the maximum and minimum values of $R$ was less than 3% of the average value.

### 2.2. Confocal Raman microspectroscopy

Raman spectra on coextruded fibers were collected in the back scattering geometry with an Olympus microscope (objective lens × 100) coupled with a Jasco NRS-2000c triple monochromator (focal length of 400 mm and diffraction grating of 1800 lines/mm) and with a nitrogen-cooled (−110°C) CCD detector (1100 × 380 pixels). The instrument was equipped with a video camera for visual examination of the specimen surface at the laser focusing spot. The 488.0 nm line from a Coherent Radiation (Innova 70) mixed gas laser was used as the excitation source and the laser beam intensity was 20–40 mW. All the spectra were recorded with a spectral slit width of 5 $cm^{-1}$ at different exposition times. An effective field depth between 4 and 5 μm was obtained by inserting two pinholes in the beam optical path. The first pinhole (diameter 100 μm) was placed on the laser head and the second (50 μm diameter) at the back focal plane of the microscope to limit Raman scattering from outside the laser focus. The diameter of the focusing spot on the sample surface was 1.5 μm. The distance between the front objective lens and the specimen was 230 μm, the maximum instrumental limit.

Depth profiling was performed by focusing the laser beam at increasing depths inside the specimen. The depth resolution and the zero depth position were checked by measuring the peak heights of the 465 $cm^{-1}$ band of a quartz crystal, according to the following procedure. The first approximation to the zero depth position was obtained by visually focusing the laser beam at the specimen surface. Then the beam focus was stepwise moved inward and outward the specimen surface and the peak intensity was recorded at each step. The resulting intensity profile is reported in Fig. 3. It is assumed that the scattering volume in the focused beam is approximately cylindrical, with a base diameter equal to the laser spot diameter (1.5 μm). It is also assumed that, when the laser beam is focused at the specimen surface (the first approximation to the zero depth position), only half of the scattering volume is underneath the surface. The peak intensity increases as the objective-specimen distance is decreased, since larger portions of the specimen are enclosed in the scattering volume. Fig. 3 shows that the maximum in the peak intensity is achieved when the focus is moved to 2.5 μm under the surface, where the scattering volume should be completely filled by the specimen. The peak intensity remains almost constant as the focusing depth is further increased, then it starts to decrease, as absorption effects become important. Thus, an estimate of the actual field depth can be obtained by doubling the depth value corresponding to the maximum of the scattered intensity ($2.5 \times 2 = 5$ μm). Field depth might have been obtained by different procedures. Usually, such methods rely on the computation of the full-width-at-half-maximum (FWHM) of the intensity profile, obtained by moving the focal plane inward and outward the sample surface. However, the choice of the FWHM as an estimate of the field depth is not completely justified in Raman scattering [27]. The method used in the present work removes this problem, but it can be biased by refraction effects at the air–sample interface. Difference in the refraction indexes of the two media leads to a systematic increase in the focus diameter as depth is increased. In the confocal optical arrangement, an appropriate choice of the pinhole can significantly reduce scattering from this excess volume. A comparison of the value of 5 μm with the field depth of 1.8 μm, obtained by the FWHM procedure, shows that the method used in the present work provides a more conservative and, likely, a more reliable estimate of the field depth.

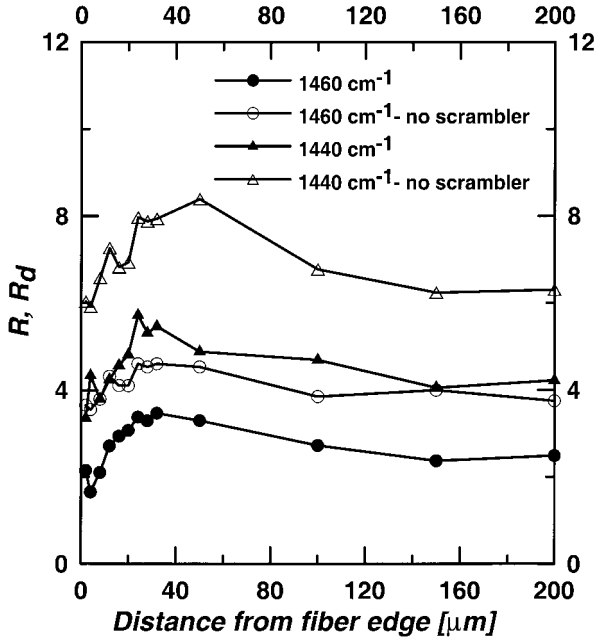


Fig. 4. Comparison of the orientation profiles in a coextruded film of solution grown single crystal mats. Profiles were obtained by two different experimental settings, with a scrambler ($R = I_{X(YX)Y}/I_{X(ZZ)Y}$; ●, ▲) and without a scrambler ($R = I_{X(YY)X}/I_{X(ZZ)X}$; ○, △).

Finally, the effects of possible biases stemming from absorption, optical inhomogeneities and surface roughness were tested by repeating the above-described procedure on a compression-molded plate of PE (IUPAC I, ST 460/10693-91). The resulting value of the depth resolution was the same, as the one measured with the quartz crystal.

In CRM, the major experimental limit to the evaluation of depolarization factors arises from the high-intensity losses due to the insertion of a scrambler. Measurement accuracy becomes insufficient when the laser beam is focused at 30 μm below the specimen surface. In these conditions, the time required to record a spectrum increases up to 25 h. Thus, the instrumental assembly was modified by removing the scrambler and by inserting an analyzer before the triple monochromator. The direction of maximum efficiency of the analyzer was maintained constantly parallel to the direction of maximum efficiency of the monochromator gratings.

Spectra were recorded at 13 different depths below the specimen surface (2,3,4,5,6,7,10,15,20,35,50,100 and 200 μm). At each depth, two different scattering geometries were used (Fig. 2, bottom). The external orthogonal reference frame is *OXYZ*, with the fiber axis always parallel to *OZ*. *OX* is in the direction of both the incident laser beam and scattered radiation (backscattering). *OY* is normal to *OZX* plane. This arrangement was used in the first measure. In the second one, the fiber was rotated by 90° around the *OX* axis, so that both the polarization direction of the half-wave plate and the direction of maximum efficiency of the analyzer were now parallel to *OZ* (Fig. 2, bottom).

Values of the normalized peak intensity ratios, $R_d(= I_{X(YY)X}/I_{X(ZZ)X})$, were plotted against the focusing depth, to estimate the orientation of the different phases along the fiber section. However, it must be pointed out that such intensity ratios do not strictly correspond to the depolarization factors. The most serious biases stem from the removal of the scrambler and from the rotation of the fiber, since small changes in the position of the focusing spot on the sample surface cannot be avoided when the specimen is rotated. The effects of changes in the spot position are partly reduced by taking measurements at different positions along the fiber axis. Each value of $R_d$ reported in this work is actually the average of at least three measurements taken at different but equivalent positions for each fiber. Results of this check showed that $R_d$ values are highly reproducible.

Experimental biases related to scrambler removal were checked by measuring values of $R_d$ on the fiber obtained by coextrusion of solution-grown single-crystal mats. The smooth and flat surface of this fiber allows measurements of the depolarization factors with the laser beam constantly focused on the surface. Orientation profiles can be obtained by moving the focusing spot from the outer border towards the fiber axis. Thus, it is possible to compare, for this same fiber, values of $R_d$ (without the scrambler) and values of $R$ measured with the scrambler. The corresponding orientation profiles (Fig. 4) display quite similar trends for different Raman bands of PE. It can be concluded that the instrumental setting used in CRM experiments does not alter the physical relevance of the orientation profiles reported in the next sections.

### 2.3. WAXS

WAXS measurements of the crystal orientation were performed on a Rigaku diffractometer by using CuKα radiation. The tube was powered at 40 kV and 40 mA. Two crossed receiving slits were used with angular widths of 3° (vertical) and 5° (horizontal), respectively. The symmetrical transmission scattering geometry was used. Well-resolved reflections from both the orthorhombic and the monoclinic phases were observed. Orientations of these two phases were measured by mounting the specimens on a fiber attachment with the draw axis normal to the incident X-ray beam. The scattering angle, $2\theta$, was set to the maximum intensity of the (100) reflection for the monoclinic and of the (110) reflection for the orthorhombic phase. Scattered intensities were recorded while rotating the specimen around the normal to the draw axis, viz. along the $\chi$ angle, for 360° at a speed of 10°/min. The sampling step size was 0.2°. For each fiber, the percent degree of preferred orientation $f$ for the two equatorial reflections was computed as [28]:

$$f = 100(180 - W_{hk0})/180$$

where $W_{hk0}$ is the integral width of the (*hk0*) reflection in

Table 2
Classification and assignments of Raman bands in PE ($\nu$ = stretching; $\nu_{as}$ = antisymmetric stretching; $\nu_s$ = symmetric stretching; $\nu_t$ = twisting; $\nu_r$ = rocking; $\nu_w$ = wagging; $\delta$ = bending)

| Observed Raman shift ($\Delta\nu$) ($cm^{-1}$) | Mode | Phase | Species [30] |
|---|---|---|---|
| 1064 | $\nu_{as}$(C–C) | Crystalline [34] + amorphous *trans* [7,13] | $B_{2g} + B_{3g}$ |
| 1080 | $\nu$(C–C) | Amorphous [13,33,34] | – |
| 1131 | $\nu_s$(C–C) | Crystalline [34] + amorphous *trans*[7,13] | $A_g + B_{1g}$ |
| 1170 | $\nu_r(CH_2)$ | Crystalline [34] + amorphous [13] | $A_g + B_{1g}$ |
| 1297 | $\nu_t(CH_2)$ | Crystalline [13,34] | $B_{2g} + B_{3g}$ |
| 1303 | $\nu_t(CH_2)$ | Amorphous [33,34] | – |
| 1370 | $\nu_w(CH_2)$ | Crystalline + amorphous [32] | $B_{2g} + B_{3g}$ |
| 1418 | $\delta(CH_2)$ | Crystalline [33,34] | $A_g$ |
| 1440 | $\delta(CH_2)$ | Amorphous *trans* (interphase) [33,34] | $A_g + B_{1g}$ |
| 1460 | $\delta(CH_2)$ | Amorphous [33,34] | $A_g + B_{1g}$ |

degrees and 180 is the $\chi$-range (degrees) used to compute $W_{hk0}$.

## 3. Results and discussion

### 3.1. Raman macrospectroscopy

The Raman spectrum of PE has been largely investigated and correlations between internal vibrational modes and observed bands have been published [29–32]. The assignment of Raman bands to the different phases in semicrystalline PE samples has been the object of extensive studies too [7,13,33–35]. Table 2 lists the Raman wavenumbers of some of the more significant bands, their internal vibrational modes and the most common assignments to the different phases. The band at 1418 $cm^{-1}$ corresponding to the methylene bending vibration ($\delta(CH_2)$), has been unanimously attributed to the crystalline phase. Experimental evidence shows that this band stems from the splitting in two components of the methylene bending vibration under the effect of the crystal field when the unit cell is occupied by two structural units [30,33,34], as in the orthorhombic and monoclinic lattices. In contrast, attribution of other bands exclusively to the amorphous or the crystalline phase is still a matter of discussion [7,13,33,34]. Difficulties seem to concentrate on the following points: (i) both crystalline chains and amorphous chain segments in an all-trans conformation may contribute to the intensity of a specific band, (ii) identification of spectral features attributable to an interphase or interfacial region, and (iii) identification of Raman bands corresponding to the amorphous liquid-like phase.

It has been reported [33,34,36] that a simple two-phase model (crystalline + amorphous) does not provide a complete description of all the features observed in PE spectra. The presence of an additional intermediate phase (interphase), where chain segments have a preferred *trans*-conformation without showing regular lateral packing, has been confirmed by Raman [33,34,36], small angle X-ray scattering (SAXS) [37] and NMR measurements [38]. Such an interphase is preferentially located at the crystallite fold surface boundary [33,37,39], and it has been associated to the presence of chain loops and entangled chain segments in this region [24,39]. Different points of view have been reported on the reliability of quantitative estimates of the interphase content by Raman [35,40,41]. However, correlations between the amount of this intermediate phase and the maximum ductility of PE rector powder samples have been

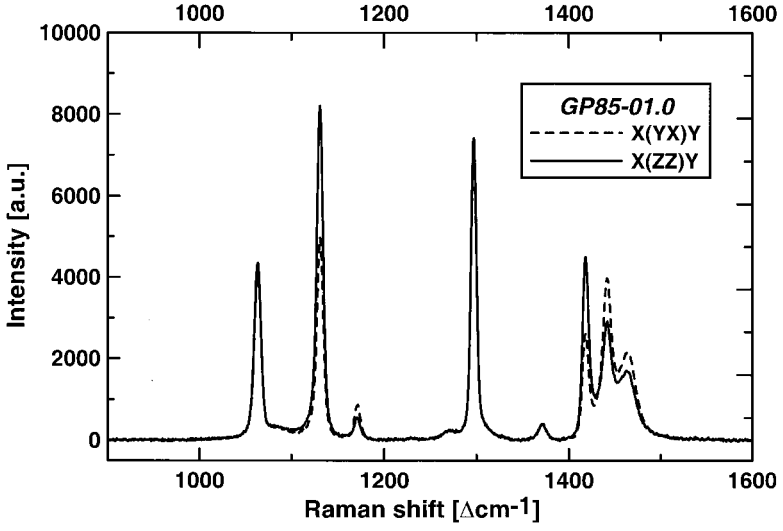


Fig. 5. Polarized Raman spectra (macrospectrometry) for the *X(ZZ)Y* and the *X(YX)Y* scattering geometries.

Table 3
Comparison of orientation properties of coextruded fibers (macrospectrometry)

| Sample identification | $f_{ortho}$ (WAXS) | $f_{mono}$ (WAXS) | $R (= I_{X(YX)Y}/I_{X(ZZ)Y})$ | | | | | | |
|---|---|---|---|---|---|---|---|---|---|
| | | | 1064 ($cm^{-1}$) | 1131 ($cm^{-1}$) | 1170 ($cm^{-1}$) | 1297 ($cm^{-1}$) | 1418 ($cm^{-1}$) | 1440 ($cm^{-1}$) | 1460 ($cm^{-1}$) |
| SI30-05.9 | – | – | 0.85 | 0.34 | 2.22 | 0.85 | 0.28 | 1.92 | 1.55 |
| SI30-12.4 | 84.7 | 84.7 | 0.94 | 0.41 | 2.43 | 0.93 | 0.36 | 1.91 | 1.63 |
| SI85-00.9 | – | – | 0.86 | 0.41 | 1.97 | 0.87 | 0.38 | 1.62 | 1.37 |
| SI85-02.0 | – | – | 0.88 | 0.39 | 2.20 | 0.89 | 0.36 | 1.72 | 1.46 |
| SI85-04.8 | 84.5 | 84.7 | 0.91 | 0.38 | 2.25 | 0.90 | 0.34 | 1.87 | 1.51 |
| Gp85-00.2 | 81.8 | 82.6 | 0.90 | 0.57 | 1.47 | 0.91 | 0.55 | 1.32 | 1.22 |
| Gp85-01.0 | 82.5 | 82.4 | 1.01 | 0.64 | 1.69 | 1.00 | 0.61 | 1.45 | 1.34 |

obtained [18,24], showing that higher amounts of the interphase actually correspond to lower ductility.

Fig. 4 shows two typical Raman spectra in the macro optical setting for the two scattering geometries *X(ZZ)Y* (full line) and *X(YX)Y* (dotted line). Bands at 1131, 1170, 1418, 1440 and 1460 $cm^{-1}$ display the most significant changes in intensities as the scattering geometry is changed. In the forthcoming discussion, we will focus mainly on the analysis of the $\delta(CH_2)$ modes, following the approach described in Refs. [12,33,34]. Comparison of PE spectra in the crystalline and molten state supports the attribution of the 1460 $cm^{-1}$ band to a liquid-like amorphous phase while the 1440 $cm^{-1}$ mode has been assigned to the interphase [33,34]. Contributions from the crystalline phase to these bands have been reported [35]. However, the opposite behavior of the depolarization factors in Figs. 6 and 7a and b suggests that such contribution is negligible for coextruded fibers.

The feature at 1080 $cm^{-1}$, which has been used by others to analyze the behavior of the amorphous liquid-like phase, is barely detectable in our spectra (see Fig. 5). The magnitude of the errors involved in the evaluation of depolarization factors from this band is too high and it will not be used in this work.

PE crystallizes normally in the orthorhombic system. The unit cell contains two independent monomers. The chain axis is parallel to the *c*-axis of the unit cell and the symmetry of the space group is $D_{2h}$. Drawn PE samples show also monoclinic crystals, where the chain axis is parallel to the *b*-axis of the monoclinic cell (*b*-unique axis) [43]. In uniaxial orientation with cylindrical symmetry (drawn fiber specimens), chains are preferentially oriented along the draw direction *Z*. This is the direction of the crystallographic *c*-axis ($c \parallel Z$) while the other axes show random orientation about this direction [7]. In an oriented specimen, the angular distribution of intensity and polarization of Raman scattered radiation are related to its degree of orientation. A general theory and experimental procedures have been developed to determine orientation parameters, by measuring intensities scattered by fiber specimens in different geometric arrangements [11,13,42]. Such intensities are related to the elements of a second rank tensor $\alpha$, the derived polarizability tensor [11].

However, in view of a comparison between Raman macro and CRM data, a simplified, although less precise, approach will be used in the present work. Thus, according to the procedure reported by Luu et al. [12], it is assumed that the orientation of the polymeric chains around the draw axis can be described by the $\alpha_{xz}$, $\alpha_{zz}$ and $\alpha_{xy}$ components of the derived polarizability tensor. It is also assumed that (Fig. 2)[1]:

$$I_{X(ZX)Y} \approx \overline{\alpha_{xz}^2}; \qquad I_{X(ZZ)Y} \approx \overline{\alpha_{zz}^2}; \qquad I_{X(ZX)Y} \approx \overline{\alpha_{xy}^2}.$$

[1] In Luu's notation $I_{X(ZX)Y} = i_{\perp}$, $I_{X(ZZ)Y} = I_{\perp}$, $I_{X(YX)Y} = i_{\parallel}$.

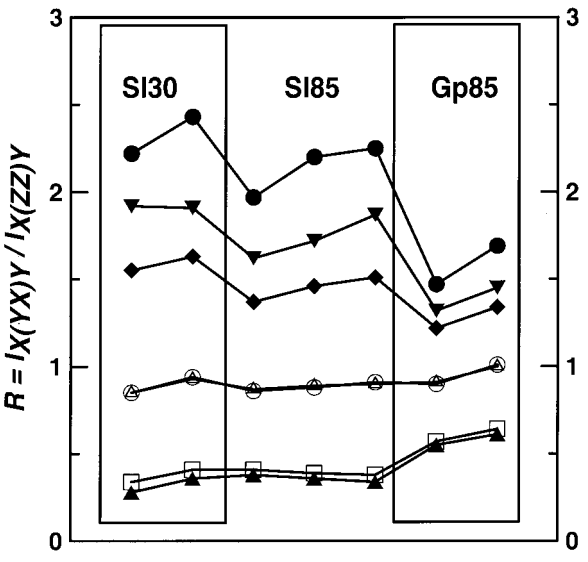


Fig. 6. Raman macrospectrometry: depolarization factor ($R$) as a function of synthesis conditions. From left to right the sample sequence is the same as in Table 1. ○: 1064 $cm^{-1}$, □: 1131 $cm^{-1}$, ●: 1170 $cm^{-1}$, △: 1297 $cm^{-1}$, ▲: 1418 $cm^{-1}$, ▼: 1440 $cm^{-1}$, 1460 $cm^{-1}$.

Orientations of the different phases can be evaluated by the corresponding depolarization factors, $R = I_{X(YX)Y}/I_{X(ZZ)Y}$. According to the above reported relationships and the scattering geometries in Fig. 2, values of $R$ range from 0 for perfect alignment around the draw axis ($Z$) to 1, for random orientation along $Z$. Then $R$ increases from 1 up to infinity, for chain alignment normal to the draw axis.

Table 3 reports values of $R$, obtained by Raman macrospectrometry measurements. Results in this table show that the crystalline components (1418 and 1131 $cm^{-1}$ bands) are well aligned parallel to the draw axis. In contrast, both the interphase (1440 $cm^{-1}$) and the amorphous phase (1460 $cm^{-1}$) display orientation normal to the draw direction, a result that has been reported previously [12] and which will be discussed later. The purely crystalline band at 1418 $cm^{-1}$ displays a degree of orientation slightly but systematically higher (lower $R$-values) than the band at 1131 $cm^{-1}$. This supports the suggestion that the 1131 $cm^{-1}$ band embodies contributions from both the crystalline phase and from amorphous chain segments in an all-*trans* conformation, like tie-molecules.

Data in Table 3 and Fig. 6 show that for each set of synthetic conditions, the degree of orientation (normal or parallel to the draw axis) increases as the molecular weight is increased. Moreover, such a correlation can be extended to the whole set of samples, with the exception of the Gp85-01.0 fiber. This trend can be attributed to a decrease in the relative concentration of chain end segments in the non-crystalline phase with respect to tie-molecules as the molecular weight is increased. At low draw ratios, tie-molecules are important as stress transfer points [4,44]. Thus, an increase in their concentration can improve the efficiency of draw, leading to higher degrees of orientation.

Inspection of data in Tables 1 and 3 and in Fig. 6 does not show any well-defined correlation between depolarization factors and powder ductilities. Samples synthesized by a gas-phase process display the lowest degrees of orientation that correspond to intermediate values of the TDR. In contrast, the highest degrees of orientation are obtained with the less ductile samples; viz. powders synthesized by a slurry process at 30°C. A possible explanation for these trends is proposed in a following section on models for draw.

### 3.2. WAXS

WAXS patterns of coextruded fibers show the simultaneous presence of reflections characteristic of both the monoclinic and the orthorhombic phase. The formation of the monoclinic phase in drawn PE samples has been associated to a martensitic transformation induced by shear forces acting normal to the chain axes and along the (*hk0*) crystallographic planes [43,45]. However, for PE the presence of the monoclinic phase cannot be uniquely associated to draw. In fact, monoclinic crystallites have been detected also in the precursor reactor powders where no macroscopic draw has ever been applied [20]. Reactor powders display a relatively high degree of crystallinity [21], but no regular mesoscopic organization, like spherulites and lamellar stacking, was observed. Moreover, SAXS profiles were consistent with the scattering produced by a polydisperse ensemble of particles having approximately globular shape [17]. Significant amounts of monoclinic crystals were detected only in reactor powders synthesized at 30°C [20], but, for all powders, neither the crystalline nor the amorphous phases display any evidence of preferred orientation. After the powder compression stage, the globular mesoscopic structure is preserved and no regular stacking of crystalline lamellae was observed [17]. As expected, at this stage, the nascent monoclinic crystallites are converted to orthorhombic, by unconstrained thermal treatment at 120°C (see Section 2). In contrast, coextrusion at 120°C has a major effect on the organization of the crystalline phase. All the fibers investigated in this work give SAXS patterns with well-defined interference peaks, indicative of regular lamellar stacking [4]. Monoclinic crystallites appear again in the system after this stage because of the martensitic process induced by draw. Coextrusion temperature is well above the transition range (70–80°C) for the conversion of monoclinic to orthorhombic. Thus, the presence of monoclinic crystals at 120°C should be related to the transverse orientation of the interphase and the amorphous phase. Such orientation is likely indicative of permanent stresses parallel to the crystallite fold surface leading to the formation of monoclinic crystallites.

Values of the percent degree of preferred orientation, $f$, for some of the fibers studied in this work are reported in Table 3. The two main equatorial reflections for both the monoclinic (100) and the orthorhombic (110) phase have been studied. Due to the geometrical relationships among

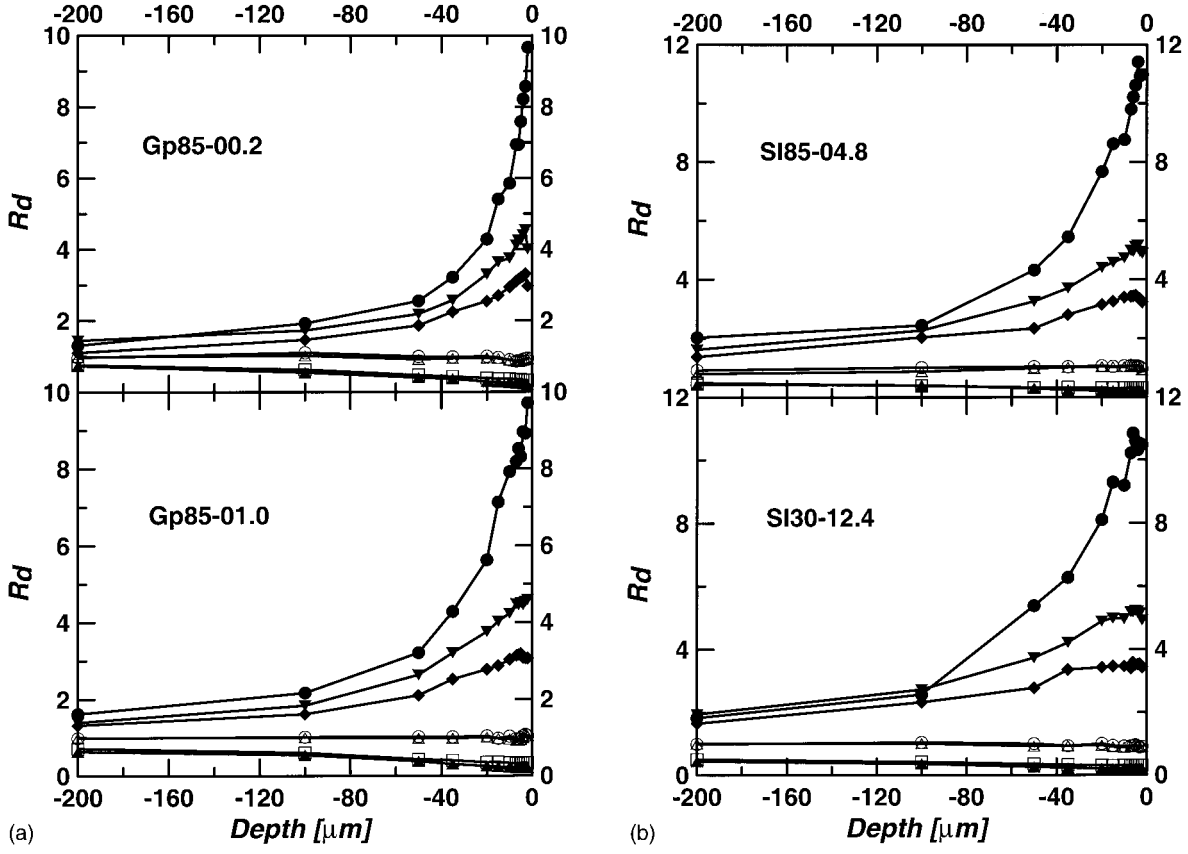


Fig. 7. (a) Intensity ratios ($R_d$) from CRM for samples Gp85-01.0 and Gp85-00.2. Symbols for the different orientation profiles as in Fig. 6. (b) Intensity ratios ($R_d$) from CRM for samples Sl30-12.4 and Sl85-04.8. Symbols for the different orientation profiles as in Fig. 6.

the crystallographic axes of the unit cells, equatorial reflections can provide information also on the orientation of the polymeric chain backbone with respect to the draw axis [7,46]. Table 3 shows that the orientations of both the orthorhombic and monoclinic phases are identical.

### 3.3. Confocal Raman microspectroscopy

Information on possible orientation profiles across the fiber section can be obtained from the CRM spectra recorded at different depths. As reported in Fig. 7a and b, plots of $R_d(= I_{X(YY)X}/I_{X(ZZ)X})$ vs. the focusing depths lead to defined trends. Oscillations of $R_d$-values at focusing depths close to zero can be attributed to the roughness of the fiber surface and to the partial filling of the scattering volume by the specimens.

From data in Fig. 7a and b it can be observed that bands, corresponding to the interphase and to the disordered amorphous phase, display significant decreases in their $R_d$-values as the focusing depth is increased. In contrast, $R_d$-values of the crystalline bands display much less significant changes and are almost constant for sample synthesized by the slurry process. This suggests that the orientations of both the interphase and the amorphous are strongly dependent on the distribution of stresses along the fiber radius during the coextrusion process, while such dependence is less important for the crystalline phase. Moreover, both the interphase and the amorphous phase are highly oriented normal to the draw direction at the fiber surface, but this effect is largely reduced towards the fiber core. Data in Table 3 and Figs. 6 and 7a and b also show that, for these two phases, synthesis in the gas phase correspond to lower values of $R_d$ close to the fiber surface.

### 3.4. Mechanisms of chain orientation on draw

The morphology and structure of drawn and ultra-drawn PE fibers have been widely investigated and several models for chain deformation have been proposed [19,44,47,48]. Correlations between processing conditions and modifications induced in the topology of the polymeric chains have been studied, especially for the initial and final stages of SSD and for a range of starting morphologies, such as melt-crystallized samples, reactor powders, single crystal mats and gel-spun fibers [49]. The stress–strain curves of highly ductile semicrystalline polymers usually display a stress yield point, which is associated to the onset for crystallite buckling [25]. The relative elongation at this point

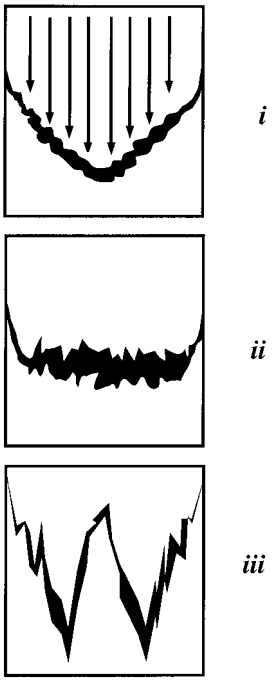


Fig. 8. Typical deformation profiles on coextrusion as obtained from the displacements of the pre-imprinted ink marks on the fiber precursor.

would correspond to a 'natural draw ratio', which, for PE, has a value of ~6, depending on composition and morphology [25]. Solid-state NMR experiments on a broad set of different polymers have proved that the existence of a crystalline α-relaxation is a structural necessary condition for ultradrawability [48,50]. At high draw ratios, chain-extended macroconformations become the dominant structural feature, when substantial chain alignment is achieved and the macroscopic elongation results in the deformation of covalent bonds and bond angles along the chain backbone. The degree of entanglements is considered the controlling factor for ultra-drawing, since complete extension of polymer chains cannot be achieved in the presence of such physical constraints. However, results in the literature do not agree on the importance of different processes such as tie-molecule extension [44], simultaneous melt-recrystallization [51], development of physical constraints for chain extension related either to entanglements [3] or to disordered crystal fold surfaces (latent entanglements) [19].

Orientation profiles can provide useful information on the structural changes associated with the above listed processes. Data reported in Fig. 7a and b show that, on coextrusion, the stress field across the fiber section is not constant, in agreement with data on deformation profiles. Such profiles have been studied by the displacement of imprinted ink marks after coextrusion (see Fig. 1). Fig. 8 reports three of the shapes that are more frequently observed [5]. A discussion of the correlations among processing conditions, molecular parameters and profile shapes led to the conclusion that the stress field on the coextruded fibers has a distinct shear component [5,6]. This conclusion can be extended to the fibers studied in the present work since the shape of the deformation profiles is similar to those of type ii in Fig. 8, even if most of the details have been blurred by ink diffusion.

In a preceding section, it has been reported that depolarization factors of both the interphase and the amorphous liquid-like bands show that these components are preferentially oriented normal to the draw direction. Similar results have been reported previously [7,12,46,52] and have been interpreted by molecular dynamics simulations [53]. Results of these simulations show that, in the initial stages of draw, the confinement of amorphous chain segments between the chain fold surfaces of two contiguous crystallites may force such segments to orient normal to the chain axes in the crystallites (Fig. 9a). Data reported in the previous section suggest that this concept can be extended to include several aspects of the dynamics of the crystalline and amorphous phases during coextrusion.

On a mesoscopic scale, nascent reactor powders can be considered assemblies of amorphous chain segments and crystallites disorderly packed into globular aggregates [17]. On drawing, amorphous chains are more easily deformed and oriented because of uncorrelated motions of individual chain segments. In contrast, chains in the crystal bodies and in the fold surfaces must move cooperatively by effect of the binding forces of the crystals. Thus, in the early stages of SSD individual structural units in the crystalline phase can be considered as made up by elongated aggregates of chain segments, similar to those reported in Fig. 9a–c. In these figures, three possible dynamics are proposed for the orientation of crystallites and non-crystalline chains on coextrusion. Fig. 9a reports the effect of the compressive force in the draw direction: confinement of polymeric segments between adjacent crystallites [53] is the dominant feature. Fig. 9b shows crystallite tilting and alignment as a result of the net torque produced by the shear stress field. The deformation induced by this process should be more important for the flexible chain segments in the folded loops and in the interphase, increasing the orientation of these components along the normal to the chain axes in the crystallites. Fig. 9c shows the effects of lateral forces, arising from the pressure gradient induced by changes in the flow rate across the fiber. The resulting displacements may induce some degree of transverse orientation in the chain segments of the folded loops and of the interphase. Complex motions, stemming from shearing and compressive effects, can be analyzed by combining the three mechanisms in Fig. 9a–c.

The above-discussed model relies on the assumption that, on coextrusion, the stiff central crystalline component is not substantially deformed. Thus, shear buckling of nascent crystallites should be negligible at this stage of SSD. Fig. 7a and b show that at EDR ~6 the orientation of the crystallites across the fiber is uniform, with the possible exception of a thin surface layer. Orientation gradients in the crystalline phases may arise from the deformation and

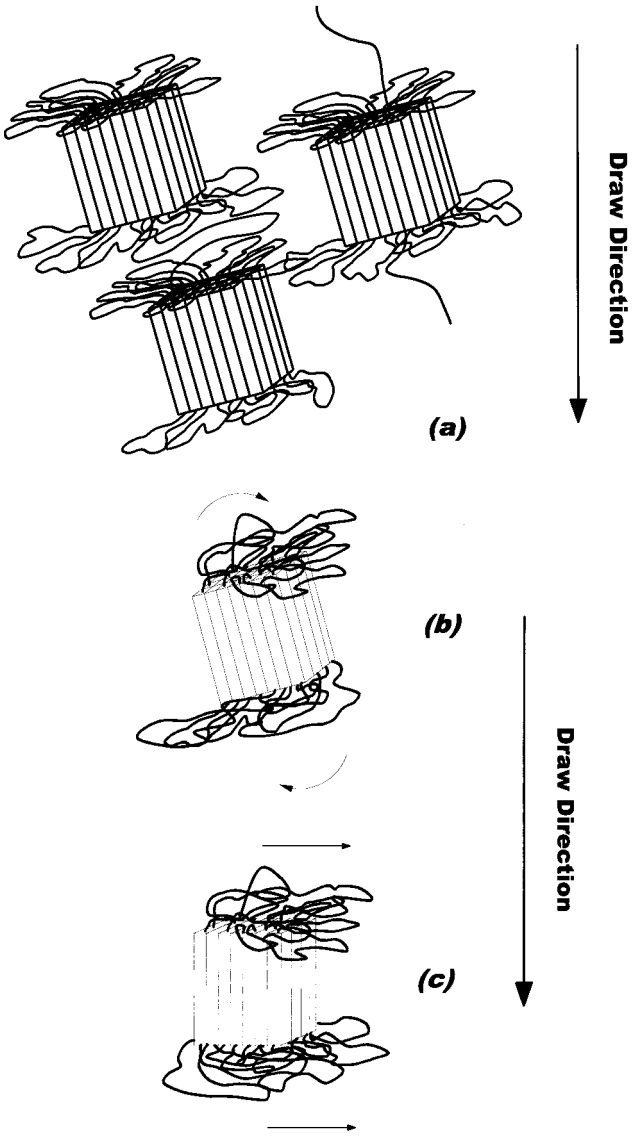


Fig. 9. (a) Chain confinement in the intercrystalline layers between adjacent crystallite boundaries. (b) Chain orientation in the intercrystalline layers by torque stemming from the shear field. (c) Chain orientation in the intercrystalline layers by lateral displacement.

the shear buckling of crystals, followed by chain unfolding of nascent crystallites. Higher degrees of orientation for these split crystals would be expected. In contrast, the orientation profiles of the crystal bands are practically flat (Fig. 7a and b), leading to the conclusion that no substantial degree of crystal buckling was achieved.

In bulk PE crystals, conversion of the orthorhombic into the monoclinic phase is a martensitic transformation, involving the slippage by shear stresses of crystallographic planes that are parallel to the chain axes [45]. For higher stresses, the same mechanism will lead to crystal buckling and higher degrees of orientation. In contrast, the almost equal values of the monoclinic and orthorhombic orientation support the conclusion that samples have not yet undergone any extensive crystallite splitting. Thus, on coextrusion at EDR ~6, nascent folded crystallites are largely preserved, a result that is consistent with the concept of 'natural draw ratio' and with the value reported for PE [25].

The dynamics reported in Fig. 9a–c may provide an explanation for the higher $R_d$-values at the fiber surface of the band at 1440 $cm^{-1}$ (interphase) as compared to the corresponding $R_d$-values of the band at 1460 $cm^{-1}$ (amorphous). Portions of the chains that are separated from the crystallite surface by increasing numbers of monomeric units, are less subject to the constraints imposed by the tilting and alignment of the stiff crystalline bodies in the stress field. They might align more easily along the flow lines in the draw direction. In contrast, chain segments in the interphase are strongly affected by the interactions with the near crystals and can be forced to orient towards the normal to the draw direction by a combination of the dynamics in Fig. 9a–c.

Such a combination is also consistent with the deformation profile in Fig. 8ii and the changes in the $R_d$-values reported in Fig. 7a and b. Higher compression and shear stresses at the die wall may result into higher deformations and higher orientations in the corresponding portions of the coextruded specimen. In contrast the flatter central part of the deformation profile in Fig. 8ii suggests that the shearing force is lower at the specimen core, reducing contributions of tilting and lateral displacement processes (Fig. 9b and c) to the system dynamics. Thus, lower degrees of orientation of the interphase and of amorphous chains in this portion of the specimen might be related to lower contributions from shear-related processes. In addition, the higher flow rate at the fiber core might release some of the constraints stemming from the compression/confinement of intercrystalline chains; tie-molecules would assume more extended conformations in these portions of the fibers.

Data in Tables 1 and 3 and in Figs. 6 and 7a and b can provide correlations between orientation degrees and powder ductilities. For samples synthesized by a slurry process a lower degree of orientation at EDR ~6 corresponds to higher ductility. This result agrees with a previous conclusion that, for the same value of macroscopic elongation, higher degrees of chain extension are obtained in less ductile reactor powders [4]. However, the Gp85 samples do not fit into this trend, since their lowest degrees of orientation correspond to intermediate ductilities. A satisfactory explanation for this last trend cannot be provided. Values of the depolarization factors would suggest the hypothesis that tie-molecules are more extended in these fibers, but further experimental evidence to support this hypothesis is still missing.

## 4. Conclusions

Investigations on the ductility of PE reactor powders have

focused on the correlations between synthesis conditions and ductility. The ultimate objective of these investigations is the identification of the most appropriate set of synthesis parameters for lowest degrees of entanglements. Coextruded fibers at EDR ~6 proved useful for this type of investigations. At low draw ratios nascent structures have not yet been obliterated, while some structural features, that may be related to controlling factors for ductility, have been enhanced by draw [4].

Results by Raman macrospectrometry showed that, in coextruded fibers, the crystalline phase is oriented parallel to the draw direction. In contrast, Raman bands attributed to the interphase and the amorphous liquid-like component are preferentially oriented normal to the draw direction. This result was already reported by other investigators [7,12,52] and it was related to the compression-confinement between adjacent crystallites of the amorphous chain segments in the intercrystalline layers [53]. CRM allowed estimating orientation profiles across the fiber section. Depolarization factors for the interphase and the amorphous liquid-like bands decrease significantly towards the fiber core. In contrast, at EDR ~6 depolarization factors for the crystalline phase are constant across the fiber, with the possible exception of a thin surface layer. Moreover, the degrees of orientation of both the orthorhombic and monoclinic crystals are identical. These results are consistent with the concept of natural draw ratio when tie-molecules between crystallites are extended and oriented along the draw axis, but the process of crystal unfolding has not started yet.

An attempt to describe the polymeric chain dynamics and the deformation modes on coextrusion can rely on the orientation of chain segments in the different phases during coextrusion. The orientation of the interphase with respect to the chain axis in the crystallites is consistent with the deformation mechanism proposed for the conversion from the orthorhombic to the monoclinic crystals [43,45]. The pulling action of chain segments in the interphase upon the crystallite fold surface can provide significant contributions to the shear stress on this surface. The resulting deformation along the (*hk0*) crystallographic planes, parallel to the chain axes, leads to the martensitic transformation from the orthorhombic to the monoclinic phase [45]. Moreover, the schemes in Fig. 9a–c may prove useful to discuss the molecular dynamics for the extraction of chain segments from the crystals to produce the chain extended morphologies observed at high draw ratios in PE fibers [54]. Recent investigations by solid-state NMR pointed out that the existence of a crystalline α-relaxation is a necessary condition for polymer ductility. The chain dynamics associated with such a process would consist in a sequence of helical jumps of a few atoms along the chain axis [48]. Accordingly, chain extension on draw would preferentially proceed by protrusion of crystalline stems from the crystals, a process favored by the pulling action of tie-molecules. Deformation and orientation profiles suggest that such a process would be dominant in the fiber core. At the fiber edges compressive and shearing effects seem to dominate the dynamics of draw. Likely, the shearing effect induced by the orientation of the chain segments in the interphase and the amorphous liquid-like components can be regarded as a preliminary stage in the development of crystallite deformation above the natural draw ratio. Further extension may proceed along different paths, one being the protrusion of crystalline chain bundles from the crystal surface. A second process can provide a low energy path for chain extension. Crystallites split into smaller blocks that are subsequently incorporated into skewed microfibrils [44]. Recursive splitting would result into extensive peeling of chain folded segments out of the crystallite bodies. Such segments are progressively extended and packed into the fibrillar aggregates that constitute the distinctive structural feature of ultra-drawn PE fibers.

## Acknowledgements

The authors wish to acknowledge the helpful discussions with Prof. Shaw L. Hsu of the University of Massachusetts on the interpretation of the Raman spectra. Authors are particularly grateful to Prof. T. Kanamoto for providing a fiber coextruded from SGC mats. In addition, the awarding of a NATO-CNR Senior Fellowship to one of the authors (S. Ottani) is gratefully acknowledged.

## References

[1] Zachariades AE, Watts MPC, Kanamoto T, Porter RS. J Polym Sci, Polym Lett Ed 1979;17:485–8.
[2] Smith P, Lemstra PJ. Colloid Polym Sci 1980;258:891.
[3] Smith P, Lemstra PJ, Booij HC. J Polym Sci, Polym Phys Ed 1981;19:877–88.
[4] Ottani S, Ferracini E, Ferrero A, Malta V, Porter RS. Macromolecules 1996;29:3292–9.
[5] Kanamoto T, Zachariades AE, Porter RS. Polym J 1979;11:307–13.
[6] Kanamoto T, Zachariades AE, Porter RS. J Polym Sci, Polym Phys Ed 1979;17:2171–80.
[7] Lafrance CP, Chabot P, Pigeon M, Prud'homme RE, Pézolet M. Polymer 1993;34:5029–37.
[8] Pereira MR, Yarwood J. J Polym Sci, Part B: Polym Phys 1994;32:1881–7.
[9] Zerbi G, Gallino G, Del Fanti N, Baini L. Polymer 1989;30:2324–7.
[10] Maxfield J, Stein RS, Chen MC. J Polym Sci, Polym Phys Ed 1978;16:37–48.
[11] Bower DI. J Polym Sci, Polym Phys Ed 1972;10:2135–53.
[12] Luu DV, Cambon L, Lapeyre C. J Raman Spectrosc 1980;9:176–80.
[13] Citra MJ, Chase DB, Ikeda RM, Gardner KH. Macromolecules 1995;28:4007–12.
[14] Hajatdoost S, Yarwood J. Appl Spectrosc 1996;50:558–64.
[15] Schrof W, Klingler J, Heckmann W, Horn D. Colloid Polym Sci 1998;276:577–88.
[16] Radder AM, Van Loon JA, Puppels GJ, Blitterswijk CA. J Mater Sci: Mater Med 1995;6:510–7.
[17] Ottani S, Ferracini E, Ferrero A, Malta V, Porter RS. Macromolecules 1995;28:2411–23.
[18] Ottani S, Porter RS. Macromol Rapid Commun 1995;16:813–9.
[19] Ottani S, Ferracini E, Ferrero A, Malta V, Porter RS. Macromolecules 1996;29:5326–31.

[20] Ottani S, Wagner BE, Porter RS. Polym Commun 1990;31:370–2.
[21] Ottani S, Porter RS. J Polym Sci, Part B: Polym Phys 1991;29:1179–88.
[22] Wang LH, Ottani S, Porter RS. J Polym Sci, Part B: Polym Phys 1991;29:1189–92.
[23] Wang LH, Ottani S, Porter RS. Polymer 1991;32:1776–81.
[24] Wang LH, Porter RS, Stidham HD, Hsu SL. Macromolecules 1991;24:5535–8.
[25] Wang LH, Porter RS, Kanamoto T. Polym Commun 1990;31:457–60.
[26] Kanamoto T, Tsuruta A, Tanaka K, Takeda M, Porter RS. Macromolecules 1988;21:470–7.
[27] Tabaksblat R, Meier RJ, Kip RJ. Appl Spectrosc 1992;46:60–68.
[28] Kakudo M, Kasai N. X-ray diffraction by polymers, 10. Amsterdam: Elsevier, 1972 (Chaps. 10 and 13).
[29] Snyder RG. J Chem Phys 1967;47:1316–60.
[30] Gall MJ, Hendra PJ, Peacock CJ, Cudby MEA, Willis HA. Spectrochim Acta 1972;28A:1485–96.
[31] Snyder RG, Hsu SL, Krimm S. Spectrochim Acta 1978;34A:395–406.
[32] Kobayashi M, Tadokoro H, Porter RS. J Chem Phys 1980;73(8):3635–42.
[33] Strobl GR, Hagedorn W. J Polym Sci, Polym Phys Ed 1978;16:1181–93.
[34] Luu DV, Cambon L, Lapeyre C. J Raman Spectrosc 1980;9:172–5.
[35] Naylor CC, Meier RJ, Kip BJ, Williams KPJ, Mason SM, Conroy N, Gerrard DL. Macromolecules 1995;28:2968–78.
[36] Mutter R, Stille W, Strobl G. J Polym Sci, Part B: Polym Phys 1993;31:99–105.
[37] Stribeck N, Alamo RG, Mandelkern L, Zachmann HG. Macromolecules 1995;28:5029–36.
[38] Choi C, Bailey L, Rudin A, Pintar MM. J Polym Sci, Part B: Polym Phys 1997;35:2551–8.
[39] Mandelkern L, Alamo RG, Kennedy MA. Macromolecules 1990;23:4721–3.
[40] Mandelkern L, Alamo RG. Macromolecules 1995;28:2988–9.
[41] Naylor CC, Meier RJ, Kip BJ, Williams KPJ, Mason SM, Conroy N, Gerrard DL. Macromolecules 1995;28:8459.
[42] Kip BJ, van Gurp M, van Heel SPC, Meier RJ. J Raman Spectrosc 1993;24:501–10.
[43] Seto T, Hara T, Tanaka K. Jpn J Appl Phys 1968;7:31–42.
[44] Peterlin A. Colloid Polym Sci 1987;265:357–82.
[45] Rault J. J Macromol Sci, Phys 1976;B12:335–71.
[46] Holmes DR, Palmer RP. J Polym Sci 1958;31:345–58.
[47] Gibson A, Davies GR, Ward IM. Polymer 1978;19:683–93.
[48] Hu W-G, Schmidt-Rohr K. Acta Polym 1999;50:271–85.
[49] Porter RS, Kanamoto T. Development of polyethylene fibers. In: Seymour RB, Porter RS, editors. Manmade fibers: their origin and development. New York: Elsevier, 1993. p. 295–302 (and references therein).
[50] Hu W-G, Boeffel C, Schmidt-Rohr K. Macromolecules 1999;32:1611–9.
[51] Chuah HH, Lin JS, Porter RS. Macromolecules 1986;19:2732–6.
[52] Read BE, Stein RS. Macromolecules 1968;2:116–26.
[53] Petraccone V, Sanchez IC, Stein RS. J Polym Sci, Polym Phys Ed 1975;13:1991–2029.
[54] Brady JM, Thomas EL. Polymer 1989;30:1615–22.